Molecular Crystals and Liquid Crystals
Publication details, including instructions for authors and subscription information:
http://www.tandfonline.com/loi/gmcl16

Static Strain Waves in Cholesteric Liquid Crystals: Response to Megnetic and Electric Fields

M. J. Press [a] & A. S. Arrott [a]
[a] Department of Physics, Simon Fraser University, Burnaby, British, Columbia, Canada, V5A 1S6
Version of record first published: 21 Mar 2007.

To cite this article: M. J. Press & A. S. Arrott (1976): Static Strain Waves in Cholesteric Liquid Crystals: Response to Megnetic and Electric Fields, Molecular Crystals and Liquid Crystals, 37:1, 81-99

To link to this article: http://dx.doi.org/10.1080/15421407608084348

Mol. Cryst. Liq. Cryst., 1976, Vol. 37, 81–99

Printed in Holland

Static Strain Waves in Cholesteric Liquid Crystals

Response to Magnetic and Electric Fields

M. J. PRESS and A. S. ARROTT

Department of Physics, Simon Fraser University, Burnaby, British Columbia, Canada V5A 1S6

(*Received August 23, 1976*)

Static strain waves appear for cholesteric liquid crystals confined between parallel plates treated to give homeotropic boundary conditions whenever the plate spacing exceeds a critical thickness which depends upon applied magnetic or electric fields. The periodicity of the strain wave varies with plate spacing and field. In practice it is possible to employ time effects to force the periodicity away from equilibrium. On a computer the periodicity can be treated as an independent variable. A three-dimensional phase diagram with plate spacing, field and periodicity as axes is studied by computer solutions of the torque equations. The director fields are described in terms of a set of parameters which allow one to visualize the complex patterns they take and how these patterns vary throughout the region of the phase diagram for which the periodic solutions exist. The fields considered are restricted to those which either force the director field to lie along the perpendicular to the plate (positive anisotropy) or to avoid that direction (negative anisotropy). The conditions for producing what are essentially field stabilized Bloch walls are described.

I INTRODUCTION

When a cholesteric liquid crystal of pitch p is contained between approximately parallel glass plates which have been treated to give the homeotropic (perpendicular) alignment of the molecules at their surfaces, there exists a critical thickness, Z_0. For plate separation, Z, less than Z_0, the only torque-free configuration is the homeotropic alignment in which the director $\hat{n}$ remains perpendicular to the glass plates (along the z-axis of a rectangular coordinate system). For plate separation larger than Z_0 there are two additional torque-free solutions which we have described previously.[1] In the simplest of these, which we have called the Translationally Invariant Cholesteric (TIC), the director field varies only in the z-direction and not in x or

y. This structure can be visualized as having the director rotating with height on a cone whose axis lies along the homeotropic axis. The half angle of this cone varies from $\theta = 0$ at the surfaces of the glass plates to some θ_{max} halfway between the surfaces. As the director rotates about this variable cone, the rate of change of the azimuthal angle with height is equal to the equilibrium wavenumber q $(=2\pi/p)$. This configuration is of lower energy than the homeotropic for $Z > Z_0$ because the saving in twist energy which results from the spiralling of the director more than compensates for the increase in the splay and bend energies caused by rotating the director away from the z-axis.

In the field-free region, the simple TIC solution is never the lowest energy configuration, at least in the one constant approximation where $K_{11} = K_{22} = K_{33} = K$. A lower energy can be achieved in a periodic structure in which the axis of the cholesteric helix is tilted away from the z-axis. This Periodic Cholesteric (PC) structure has translational invariance along one axis (y) in the horizontal plane. We have shown that this tilting of the helix increases the splay and twist energies but produces a larger decrease in the bend energy. The small net saving in energy (less than 2% with no applied field) is responsible for the striking finger-like patterns shown in Figure 1.

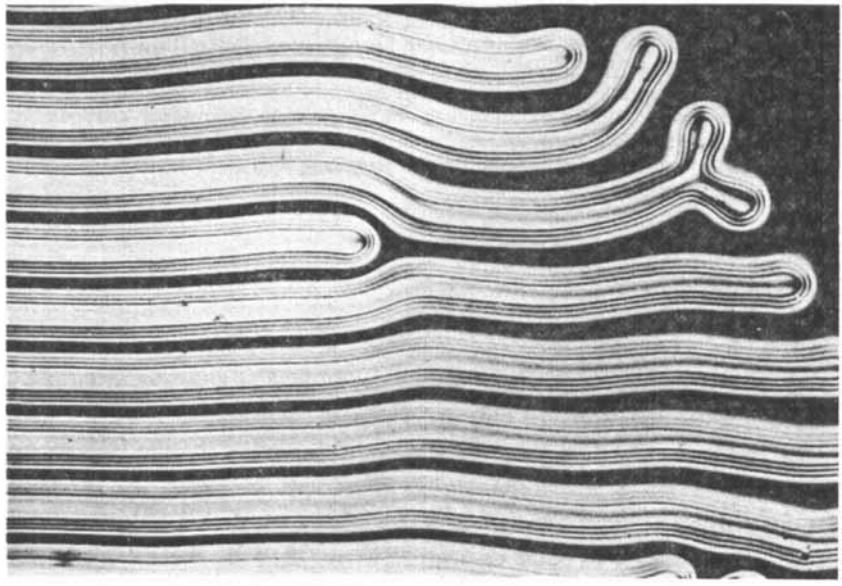

FIGURE 1 The nucleation of the fingers from the homeotropic takes place in this preparation at a cell thickness of about 20 microns with a periodicity of about 60 microns. The sample between crossed polarizers was photographed in red light.

Since the molecules comprising liquid crystals are both magnetically and electrically anisotropic we can expect to cause a reorientation of the director field in response to applied magnetic or electric fields. For most liquid crystals the magnetic anisotropy is positive, that is, the local energy density is reduced if the director aligns parallel to the applied magnetic field. On the other hand the electric anisotropy can be either positive or negative, causing the director to align parallel or perpendicular, respectively, to the applied field. The most interesting case is when the electric anisotropy is negative because then it is possible to change the external applied stimulus from a large and positive anisotropic effect on the director field (using a magnetic field), continuously through zero, to being large and negatively anisotropic (using an electric field). In this paper we will predict the response of the director field to external homeotropically ($\parallel$ z-axis) applied fields with both signs of anisotropy in the one constant model. We will also describe qualitatively our observations of the response of real liquid crystals to homeotropically applied magnetic fields. This along with the sample preparation is given in Section II. The corresponding experiments with applied electric fields have not yet been attempted. The energy and torque equations for the one constant approximation are derived in Section III (and the appendices) making use of the experimental observation that there is translational invariance (approximately) in at least one dimension parallel to the plates.

Section IV describes the response of the solutions which are translationally invariant in the x-y plane to the external applied field. We show that the critical thickness, Z_0, which in the absence of any external fields was equal to half the equilibrium pitch, now becomes a function of the applied field. When the anisotropic interaction, $\Delta\chi$, is positive, Z_0 increases as the applied field, A, is increased, whereas when $\Delta\chi$ is negative, the critical thickness decreases with increases in the applied field. Scaling relationships are obtained for the variation of the director field and the energy as a function of the plate separation and the applied field.

We then deal with the response of the PC configurations to applied fields. As the field is changed, the periodicity of minimum energy, X_0, is also changed. As long as the periodicity is unconstrained our computer calculations indicate the PC configuration remains lower in energy than the corresponding TIC configuration. However, if the periodicity is constrained theoretically there are critical fields for which the PC configuration becomes higher energy than that of the corresponding TIC and would collapse into it if allowed to by some nucleation process. These concepts are discussed more fully in Section V.

Discussion of the effects of fields in the plane of the plates is to be taken up separately.

II SAMPLE PREPARATION AND OBSERVATIONS

The samples were prepared by doping methoxybenzylidene butyanaline with small amounts of cholesteryl oleate producing cholesterics with pitches of the order of tens of microns. Glass plates were treated with the surfactant hexadecyltrimethylammonium bromide to give the homeotropic alignment of the molecules at their surfaces. The cholesteric material was sprayed on the glass plates to produce small droplets, which, when contained in an approximately parallel plate geometry with a plate separation of about 15 microns produced cylindrical droplets about 500 microns in diameter. The PC configuration then nucleated out from the boundaries of the droplet forming an array of finger-like structures which ceased growing when they filled all the available space as shown in Figure 2a.

The sample was placed in a holder between the pole tips of a specially designed water-cooled magnet with hollow pole tips that could produce magnetic fields up to 10 kG directed along the homeotropic axis of the sample and parallel to the direction of the light. The magnetic field was varied and the response of the PC configuration was observed using a Reichert metallurgical microscope. The photographs were taken in white light with the sample contained between crossed polarizers.

At first there is little change in the fingers as the magnetic field is increased slowly from zero. As the critical field (about 3–4 kG for this sample) is approached the fingers start to retreat back to the walls of the droplet, Figure 2b – 2e. This takes place first in the thinner part of the droplet (the plates from a slight wedge) because the critical field required to drive the sample homeotropic is a function of the separation of the plates. For large enough fields the whole sample is hometropic (except for the walls of the droplet), Figure 2f.

As the field is slowly lowered the fingers nucleate out from the thicker part of the cell and propagate to the thinner end, Figure 2g–2i. At zero field the usual finger pattern returns, Figure 2j. There is hysteresis in this cycling due to the exact way in which the fingers are nucleated from the walls of the droplet and from the particular way in which the magnetic field is cycled.

In the remaining pictures the field is changed very rapidly. In Figure 2k the field has been increased from 0 to 10 kG. The fingers become narrower as well as shrinking from their ends, rapidly disappearing (in the order of a few seconds), Figures 2k–2m, producing the homeotropic configuration, Figure 2n. The rest of the sequence shows the patterns resulting from the large magnetic field being abruptly turned off. The sample responds by first nucleating regions of the TIC configuration, Figure 2o, since it is much lower in energy than that of the homeotropic. The PC structure, being slightly lower in energy than the TIC, then slowly nucleates out (10 sec) producing the usual finger patterns, Figures 2p–2r.

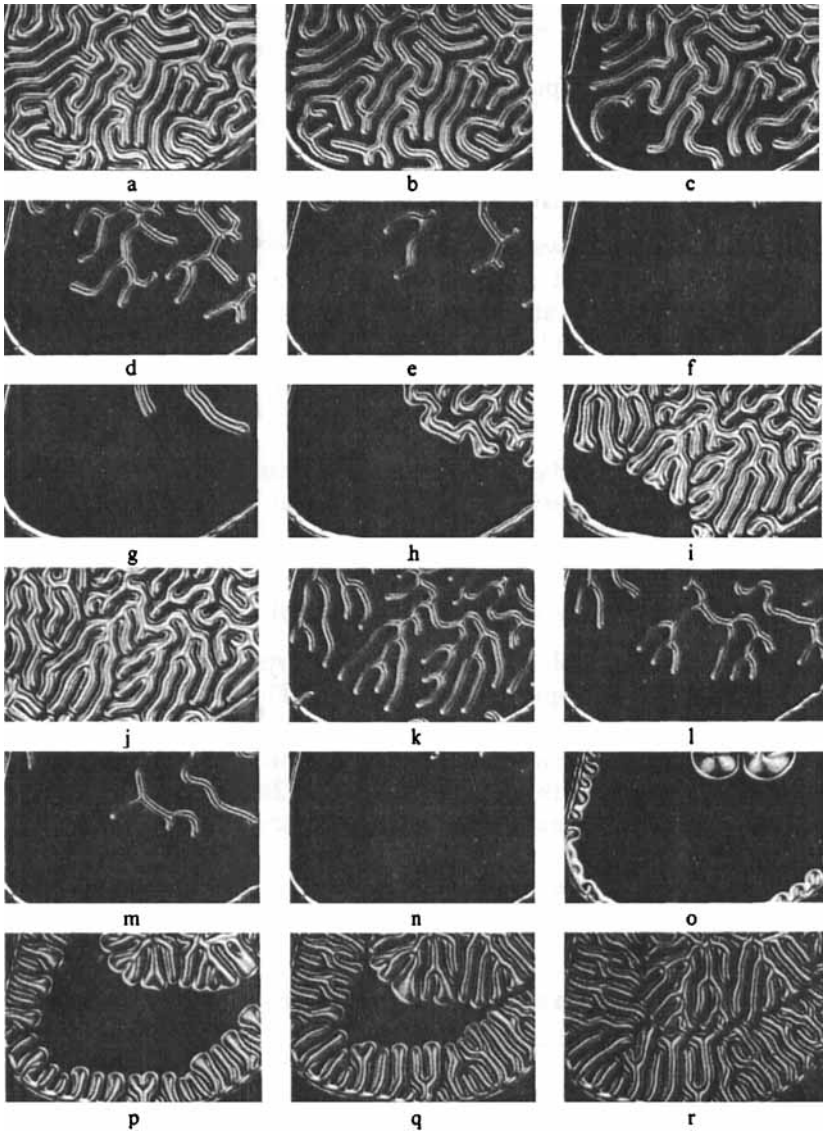

FIGURE 2 The fingers are contained in a large flat drop ($\sim$500 microns diameter) between approximately parallel plates with a separation of about 15 microns. The periodicity is about 30 microns. In (a) the magnetic field is absent. In (b)–(e) the field (applied perpendicular to the sample, i.e., out of the page) is slowly increased to the critical field, about 3–4 kG for this sample, causing the fingers to retreat from the thinner edge of the large droplet, finally disappearing for fields above the critical field, (f). In (g)–(i), as the magnetic field is slowly decreased the fingers nucleate out from the thicker part of the droplet forming the usual finger pattern at zero field, (j). In (k)–(m) the field has been rapidly increased to 10 kG. The fingers become narrower as well as shrinking from their ends, disappearing in a few seconds producing the homeotropic configuration, (n). The field is then abruptly turned off and regions of the TIC are produced, (o), which break up into the usual finger structures, (p)–(r), in about 10 seconds.

The mathematical description of these effects will be given in the remainder of this paper.

III ENERGY AND TORQUE EQUATIONS

A rectangular coordinate system is used with the z-axis perpendicular to the plates and the y-axis taken as the direction of translational invariance. The orientation of the director at a given point in space can be given in terms of the usual polar angles θ and ϕ and is written as

$$\hat{n}(z, x) = \hat{x} \sin \theta(z, x)\cos \phi(z, x) + \hat{y} \sin \theta(z, x)\sin \phi(z, x) + \hat{z} \cos \theta(z, x). \tag{1}$$

The expression for the elastic energy density per unit volume was derived previously.[1] To this expression we must add the energy density due to the presence of the applied field. With the applied field, A, parallel to the z-axis the field energy density can be written as[2]

$$f_A = -(\chi_\perp A^2 + \Delta\chi A^2 \cos^2 \theta)/2$$

where $\chi_\perp$ is the susceptibility of the molecules perpendicular to their long axes and $\Delta\chi$ is the anisotropy in the susceptibility. The term $\chi_\perp A^2$ is independent of the molecular orientation, and can be neglected. When $\Delta\chi > 0$ the energy is reduced if $\hat{n}$ is parallel to $\mathbf{A}$ ($\theta = 0$), while if $\Delta\chi < 0$ putting the director at right angles to the applied field ($\theta = \pi/2$) reduces the energy.

The energy density per unit length (in the y-direction) is given by

$$\begin{aligned} E_l = \frac{1}{2} \iint \{ & dz\, dx(K[\sin^2 \theta(\phi_x^2 + \phi_z^2 + 2 \sin \phi(\theta_z \phi_x - \theta_x \phi_z)) \\ & + \theta_x^2 + \theta_z^2 + q^2 \\ & + 2q(\sin \phi \theta_x + \sin \theta \cos \theta \cos \phi \phi_x - \sin^2 \theta \phi_z)] \\ & - \Delta\chi A^2 \cos^2 \theta)\}. \end{aligned} \tag{2}$$

The calculus of variations is used to minimize the total energy. This produces a pair of coupled, non-linear, second order, partial differential equations. These are

$$\nabla^2\theta = \sin \theta \cos \theta\left(\phi_x^2 + \phi_z^2 + \frac{\Delta\chi}{K} A^2\right) - 2q \sin \theta(\cos \theta \phi_z + \sin \theta \cos \phi \phi_x) \tag{3}$$

and

$$\sin^2 \theta \nabla^2 \phi = 2q(\sin^2 \theta \cos \phi \theta_x + \sin \theta \cos \theta \theta_z) - 2 \sin \theta \cos \theta(\theta_x \phi_x + \theta_z \phi_z) \tag{4}$$

which are to be satisfied everywhere in the bulk. At the surfaces the polar angles $\theta = 0$ while the azimuthal angles ϕ are determined by analytic extrapolation from the bulk.

This coordinate system has problems when the polar angle θ is close to zero in the bulk. We then can use a coordinate system which has been rotated by $\pi/2$ about the x-axis as described previously.[1] The equations for this coordinate system are given in Appendix A. A third coordinate system using the direction cosines α, β, and γ has proved to be advantageous. Its use requires the introduction of a Lagrange multiplier λ. The form of the α, β, γ torque equations and some comments upon their use are given in Appendix B. Not only does this system avoid any problems with poles but it also turns out to be faster to generate relaxed solutions on a computer.

The computer solution of these equations have already been discussed.[1] Briefly, since we are looking for periodic solutions we assume a repeat distance, X, and use periodic boundary conditions. The finite difference analogues to Eqs. (3) and (4) are iterated until a stable solution is found and then X can be varied to find the periodicity of minimum energy, X_0.

IV HOMEOTROPIC AND TRANSLATIONALLY INVARIANT CHOLESTERIC CONFIGURATIONS IN APPLIED FIELDS

When the derivatives with respect to x are set equal to zero in Eq. (2) the energy density per unit area in the x-y plane becomes

$$E_a = \frac{1}{2} K \int_0^Z dz \left(\sin^2 \theta \phi_z^2 + \theta_z^2 - 2q \sin^2 \theta \phi_z + q^2 - \frac{\Delta\chi}{K} A^2 \cos^2 \theta \right) \quad (5)$$

while the torque equations, Eqs. (3) and (4) reduce to

$$\theta_{zz} = \sin \theta \cos \theta \left(\phi_z^2 - 2q\phi_z + \frac{\Delta\chi}{K} A^2 \right) \quad (6)$$

and

$$\sin^2 \phi_{zz} = 2 \sin \theta \cos \theta \theta_z (q - \phi_z). \quad (7)$$

The most trivial solution to the torque equations is $\theta = 0$ which is the homeotropic configuration. For a cell thickness Z the energy per unit area of the homeotropic solution is

$$E_a^H = (Kq^2 - \Delta\chi A^2) Z/2. \quad (8)$$

When there is no applied field ($A = 0$) the energy is all twist and is proportional to the thickness of the cell, Z. As the field is increased, for $\Delta\chi > 0$, the

energy is reduced. For $\Delta\chi < 0$, the energy of the homeotropic configuration increases as the applied field is increased.

When θ is not identically zero, Eq. (7) is satisfied by

$$\phi_z = q. \tag{9}$$

Putting this into Eq. (6) gives

$$\theta_{zz} = -\left(q^2 - \frac{\Delta\chi}{K} A^2\right)\sin\theta\cos\theta. \tag{10}$$

When θ remains small this can be integrated to give

$$\theta = \theta_{\max} \sin\left(q^2 - \frac{\Delta\chi}{K}A^2\right)^{1/2} z. \tag{11}$$

Since θ must equal zero at $z = Z$ as well as at $z = 0$, the argument of the sine must go to π at $z = Z$. This defines the critical thickness

$$Z_0(A) = \pi \Big/ \left(q^2 - \frac{\Delta\chi}{K} A^2\right)^{1/2}. \tag{12}$$

There is a line on a phase diagram of field and thickness which gives the limits of the TIC configurations. It is convenient to show the phase diagram using the variables $W = \pi^2/Z^2q^2$ and $F = \Delta\chi A^2/Kq^2$ as done in Figure 3.

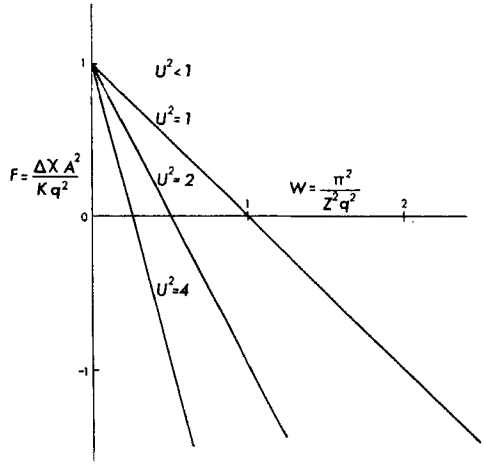

FIGURE 3 The phase diagram for the TIC configurations. For $F > 1 - W$ only the homeotropic configuration is stable. For $F < 1 - W$ the TIC is of lower energy than the homeotropic. Along lines of constant $U = Z/Z_0$ the TIC solutions scale, i.e., all solutions have the same value for $\theta_{\max}$ and the same value for ZE_a/K.

In these variables the equation of the limit of phase stability is

$$F = 1 - W. \tag{13}$$

For F greater than $1 - W$ there is no thickness for which the TIC solution exists. Solutions exist for the domain below the line $F = 1 - W$. This diagram also exhibits a scaling relation for θ_{max} and the total energy in the one constant approximation. On each straight line through the point $F = 1$ and $W = 0$ all points have the same value of θ_{max}. If we write these lines as

$$F = 1 - U^2 W \tag{14}$$

then $U^2 = 1$ is the phase boundary and for each value of $U^2 > 1$ there is a fixed value of θ_{max} all along that line. This can be seen by noting that Eq. (10) can be written as

$$\theta_{uu} = -\pi^2 \sin\theta \cos\theta \tag{15}$$

if we use the dimensionless variable $u = z/Z_0$. Thus all solutions scale with $U = Z/Z_0$. θ_{max} as a function of Z/Z_0 is shown in Figure 4.

Obviously we can talk about critical fields for fixed thickness or about critical thickness for fixed fields. For $W < 1$ and $\Delta\chi > 0$ the application of sufficient field drives the TIC to the homeotropic. For $W > 1$ and $\Delta\chi < 0$ the field can drive the homeotropic to the TIC. This latter case is like a Frederiks transition.[3]

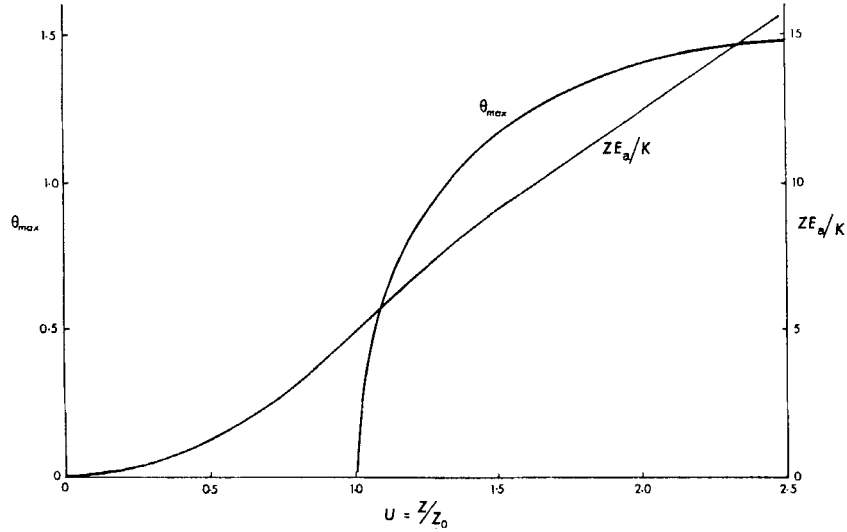

FIGURE 4 The variation of θ_{max} and ZE_a/K as a function of Z/Z_0 for the TIC configurations.

The total energy per unit area, E_a, time Z/K scales with Z/Z_0 even though the individual terms in the energy do not. ZE_a/K is shown in Figure 4. For large Z/Z_0, θ_{max} goes to $\pi/2$, ZE_a/K is proportional to Z and the energy becomes independent of Z, approaching the value

$$E_a = 2Kq(1 - (\Delta\chi A^2/Kq^2))^{1/2} \tag{16}$$

In the limit of large Z/Z_0, that is, large spacing or large fields for $\Delta\chi < 0$, θ is close to $\theta_{max} = \pi/2$ everywhere except in a boundary layer of thickness

$$\delta \equiv (\pi/2)/\theta_z(0), \tag{17}$$

where $\theta_z(0)$ is the magnitude of the z-derivative of θ at the surfaces. In the limit of large Z/Z_0

$$\theta_z^2(0) = (q^2 - \Delta\chi A^2/K) \tag{18}$$

from a first integral of Eq. (10). For $-\Delta\chi A^2/K \gg q^2$ the thickness of the boundary layer is therefore

$$\delta = \left(\frac{\pi}{2}\right)\left(\frac{K}{-\Delta\chi}\right)^{1/2}\left(\frac{1}{A}\right). \tag{19}$$

The strain energy is restricted to the boundary layer where $\theta \neq \pi/2$. There the twist energy is simply proportional to δ while the splay and bend energies[1] are proportional to $\theta_z^2\delta(0)$. The twist energy goes towards zero inversely as the applied field while the splay and bend energies increase linearly with field. The limiting energies are $E_{twist} = 0$, $E_{bend} = (2/3)(-\Delta\chi K)^{1/2}A$, $E_{splay} = (1/3)(-\Delta\chi K)^{1/2}A$, $E_{field} = (-\Delta\chi K)^{1/2}A$ and $E_{total} = 2(-\Delta\chi K)^{1/2}A$. The linear relation between energies and field comes from the product $A^2\delta$.

The scaling which appears here for the TIC solutions will not be seen for the PC solutions. Nor would it occur even for the TIC solutions if one abandoned the one constant approximation.

V PERIODIC CHOLESTERIC CONFIGURATIONS

The above calculations of the field dependence of the TIC configurations serve as an introduction to the study of the periodic cholesteric (PC) configurations. The latter we are able to observe experimentally as well as to calculate. The periodic variation in the x-direction can be visualized as a series of TIC solutions of differing θ_{max} and of a continuous change with x in the phase of the rotations with z of the ϕ-component. To carry this visualization through it is sufficient to concentrate on the behavior of the director in the mid-plane between the plates. The director at successive values of x

at $z = Z/2$ can be mapped back on a cone with its axis in the z-x plane. The cone axis makes an angle θ_{axis} with respect to the z-axis and has a half angle $\theta_{1/2}$. As we progress in the x-direction the director rotates about the cone axis while lying in the cone. The pattern between the mid-plane and the surfaces is approximated by visualizing a gradual relaxation of θ towards zero as the surfaces are approached and a rotation of the ϕ-component approximating

$$\phi(z, x) = \phi(Z/2, x) + q(z - Z/2). \tag{20}$$

All this is only an approximation in that the cone is not exactly right-circular nor does θ_{max} occur exactly at $z = Z/2$ except for particular values of x. The description is sufficiently good that one can discuss the PC solutions in terms of the variables θ_{axis}, $\theta_{1/2}$, Z and X where X is the periodicity and Z is as before the plate spacing. For any given plate spacing, Z, there will be a value X_0 for which the average energy density is a minimum. Yet on the computer and to some extent in practice one can treat X as well as Z as independent variables and enquire about the limits of stability of the PC solutions on an X-Z phase diagram. This subject has been dealt with in greater detail elsewhere.[4] Here we wish to add a third axis to the phase diagram to represent fields applied along the z-axis with $\Delta\chi$ either positive or negative as was done for the TIC configurations. Thus in addition to $F = \Delta\chi A^2/Kq^2$ and $W = \pi^2/Z^2q^2$, we introduce the variable $V = 1/X^2q^2$ as an axis out of the plane of F and W shown in Figure 3.

Obviously we can only selectively investigate such a space with the computing methods necessary to the problem. For each point F, W, V one must carry out a relaxation calculation on a grid of x and z with steps of the order of $0.2/q$.

A typical solution is that of what we term our reference state: $Z = 4.8/q$ and $X = 12.8/q$. This choice of X is very close to X_0 for $Z = 4.8/q$ and the energy for this state is lower than the energy of the corresponding TIC solution for the same Z by 2%. This is the largest percentage lowering found in zero field ($F = 0$) for any choice of $W(Z)$ and $V(X)$.

Starting with $Z = 4.8/q$ ($W = 0.45$) and applying fields with $\Delta\chi$ positive or negative we first hold X constant at $12.8/q$ ($V = 0.0061$) and observe the variation of θ_{axis}, $\theta_{1/2}$ and the energy of the solution. Then we relax X at several values of the field to find X_0 and the values of θ_{axis} and $\theta_{1/2}$ for that X_0. The energy is normalized to the value for the homeotropic solution in zero field. This removes the volume dependence of the energy and the value of the elastic constant K. We define a difference in average energy per unit volume with respect to the TIC as

$$\Delta f = \frac{E^{PC} - E^{TIC}}{E^{H}(A = 0)}. \tag{21}$$

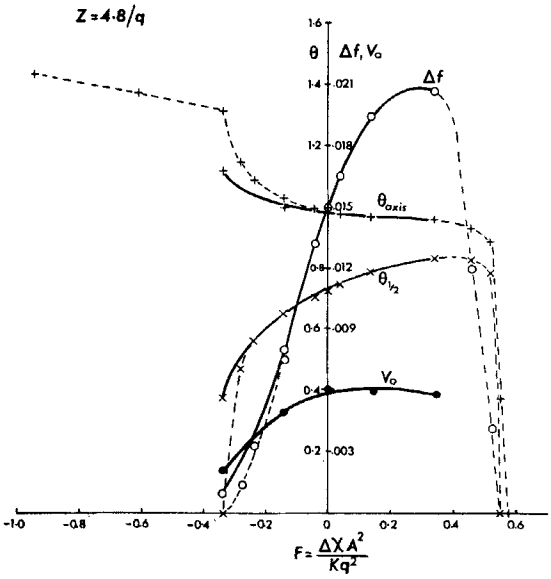

FIGURE 5 For $Z = 4.8/q$ the variation of θ_{axis}, $\theta_{1/2}$ and Δf as a function of F for the constrained (dashed lines, $X = 12.8/q$ ($V = 0.0061$)) and unconstrained (solid lines) PC configurations. Also shown is the variation of $V_0 = 1/(X_0 q)^2$ as a function of F for the unconstrained PC configurations.

The results for $Z = 4.8/q$ are summarized in Figure 5. With X constant at $12.8/q$ the application of a field with $\Delta\chi < 0$ leads to a transition to the TIC configuration for $F = -0.34$ as $\theta_{1/2}$ collapses. If X is unconstrained we believe that no such collapse will occur but rather X_0 should go to infinity ($V_0 \to 0$) as the field goes to infinity. Thus the TIC solution for large field is the limiting case for fields applied to the PC solution with $\Delta\chi < 0$.

For $\Delta\chi > 0$ the application of a sufficiently large field leads to a collapse to the homeotropic configuration. For $Z = 4.8/q$ the value of $\theta_{max} = \theta_{axis} + \theta_{1/2}$ is greater than $\pi/2$ and the field tends to increase $\theta_{1/2}$ inasmuch as the torque from the field rotates the director towards $\theta = \pi$ for some regions of the structure. Eventually the director in those regions rotates back towards $\theta = 0$ and the collapse to the homeotropic takes place. This process appears to be continuous at least for a constrained X. As X gets large the calculations become more time consuming and this discourages searches for X_0.

For values of $\pi/q < Z < 4.8/q$ we expect results similar to those for $Z = 4.8/q$ but without the rise in $\theta_{1/2}$ with field for $\Delta\chi > 0$.

We have calculated the behavior of the apparent transition to the TIC that takes place for fixed X in fields with $\Delta\chi < 0$ for a number of values of Z

including values of $Z < \pi/q$. For $\Delta\chi < 0$ and $Z < \pi/q$ increasing the field leads to an onset of the TIC solution from the homeotropic followed by a transition of the PC of the fixed periodicity and then back to the TIC. If one were to relax X we believe the TIC would not occur in this process but that X_0 would start at infinity at the critical field $F_0(z)$, go through a minimum and increase back towards infinity as $-F$ goes to infinity. The contour for the stability of the PC solutions with $X = 14.4/q$ for $\Delta\chi < 0$ is shown in Figure 6 on a phase diagram of $-F$ and W. During this process with fixed X the value of θ_{axis} starts from θ_{max} of the TIC solution and $\theta_{1/2}$ starts from zero for the transition with increasing field from the TIC to the PC and for the transition with decreasing field from the TIC to the PC. These remarks hold for $Z < 5.6/q$ ($W = 0.31$) but for $Z > 5.6/q$ the behavior is more complicated for X constrained inasmuch as one is then dealing with the over-the-pole configuration, that is solutions with $\theta_{axis} - \theta_{1/2} < 0$.

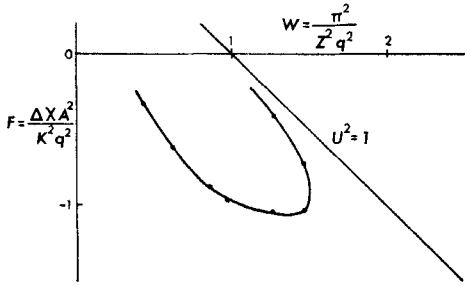

FIGURE 6 For $F < 0$, the limits of stability for the PC configurations with periodicities less than $X = 14.4/q$ is indicated by the partial contour line. The PC configurations would be stable everywhere below the line $U^2 = 1$ if their periodicities were allowed to increase toward infinity.

The behavior for $Z = 6.4/q$ has been investigated as an example of the over-the-pole behavior. For fixed X and $\Delta\chi < 0$ the application of a field flattens out the cone driving θ_{axis} towards zero and $\theta_{1/2}$ towards $\pi/2$. For an over-the-pole configuration there is no way to reach the TIC configuration as long as X is constrained. What we suppose happens is that the application of a field with $\Delta\chi < 0$ will force the periodicity towards infinity as the cone rotates with θ_{axis} going to zero and $\theta_{1/2}$ going towards the TIC solution for those values of Z and F. In such a case the application of a rather small field should produce a solution very close to the TIC solution. X_0 would be so large that we could not calculate it. Thus negative $\Delta\chi$ and $Z > 5.6/q$ are conditions under which one should be able to experimentally produce configurations very close to those calculated for the TIC.

For $\Delta\chi > 0$ and $Z > 5.6/q$ we see the full effect of those parts of the pattern where θ is greater than $\pi/2$ as the field drives those regions towards $\theta = \pi$.

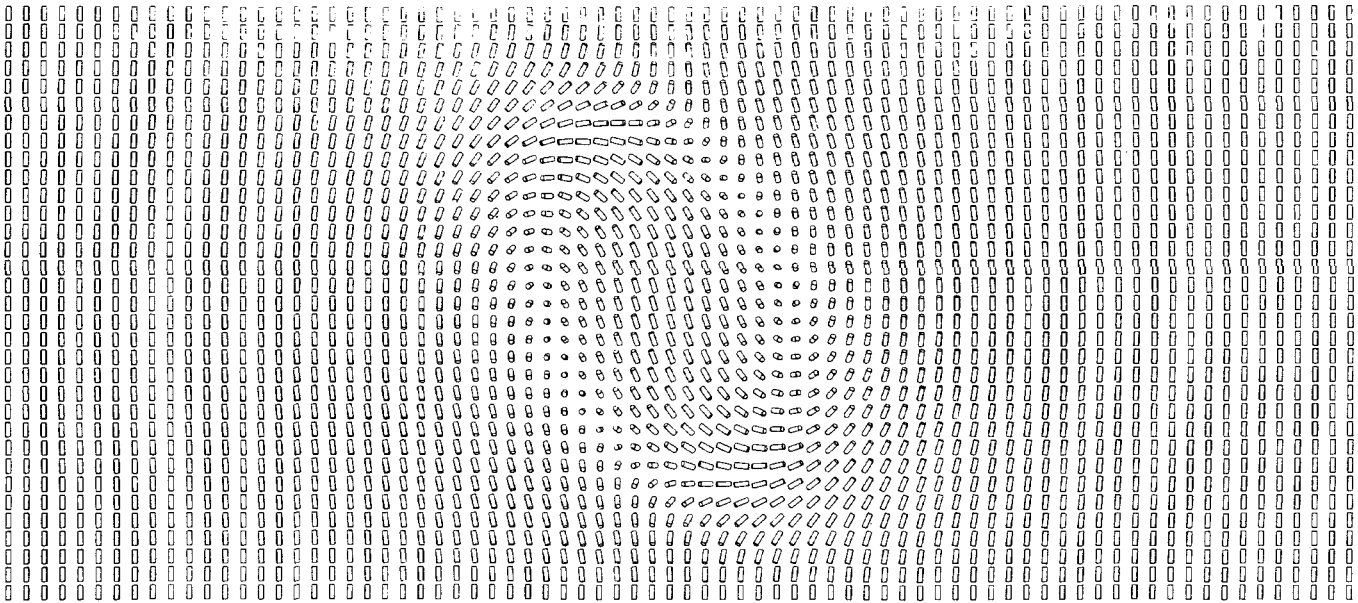

FIGURE 7 This cross-sectional view showing the 360 degree Bloch wall in one finger of the PC in an applied field $F = 1.15$ has been generated by computer for a sample of thickness $Z = 6.4/q$ and with periodicity constrained at $X = 15.2/q$.

We produce an effect in which large regions of the periodic structure are aligned with $\theta = 0$ but the periodicity shows up as what can be described as 360 degree Bloch walls, but which requires some study of Figure 7 to fully appreciate. At $X = 15.2/q$ and $Z = 6.4/q$ this 360 degree Bloch wall is stable up to $F = 1.4$ whereas the TIC solution would be stable only up to $F = 0.79$. The behavior for $Z = 6.4/q$ is summarized in Figure 8 to the extent that we have calculated it. The already large values of X have been particularly discouraging of searches for X_0 away from $F = 0$. As we believe that the values of $\theta_{1/2}$ for X_0 cannot be far from θ_{max} of the TIC solution for $\Delta\chi < 0$ we have included these in Figure 8. Note that the energy of the configuration with 360 degree Bloch walls can be greater than the homeotropic configuration energy. The collapse of the Bloch wall structure occurs when the local energy density in the center of the wall reaches the energy density of the homeotropic configuration.

When the applied field is large enough to force homeotropic alignment of the regions between the 360 degree Bloch walls the Bloch walls should be forced apart if the constraint on the periodicity is relaxed. It is likely that the process goes continuously with the periodicity reaching infinity at the field for the TIC to homeotropic transition.

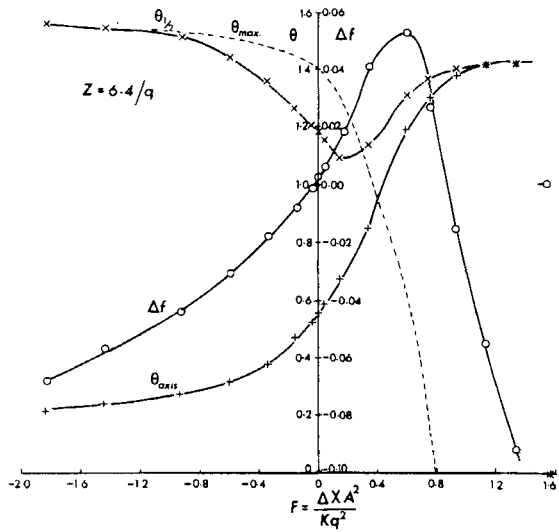

FIGURE 8 For $Z = 6.4/q$ the variation of θ_{axis}, $\theta_{1/2}$ and Δf as a function of F for the constrained ($X = 15.2/q$) PC configuration. At $F \sim 1.4$ the PC configuration collapses to the homeotropic destroying the 360 degree Bloch wall. This wall would not be created if the field were decreased from $F > 1.4$ towards 0. Also shown as a dashed line is the variation of θ_{max} for the corresponding TIC configurations.

Such a 360 degree Bloch wall should be possible in magnetism by following the procedure suggested by Hornreich.[5] If a magnetic field is applied antiparallel to the central spins of a wall of the form calculated by La Bonte,[6] which has a Néel wall rotation at the surfaces and a Bloch wall rotation at the center, then the pattern of Figure 7 should result.

VI SUMMARY

The above results indicate some of the responses to electric and magnetic fields of cholesteric liquid crystals confined between parallel plates with homeotropic boundary conditions and with fields applied perpendicular to the plates. Certain aspects of the phase diagram of plate spacing, periodicity and fields have been brought out. Using the mnemonic device of the cone formed by projecting the director fields at the midplane onto a single point, we are able to summarize a number of these findings in Figure 9.

For $W \sim 1.2$, that is, for a thickness less than the critical thickness in zero field, there is only the homeotropic solution for $F \geq 0$. For $F < 0$ the periodic solution nucleates from the homeotropic with infinite periodicity ($V = 0$). θ_{axis}, $\theta_{1/2}$ and V all then increase with field. $\theta_{1/2}$ and V go through

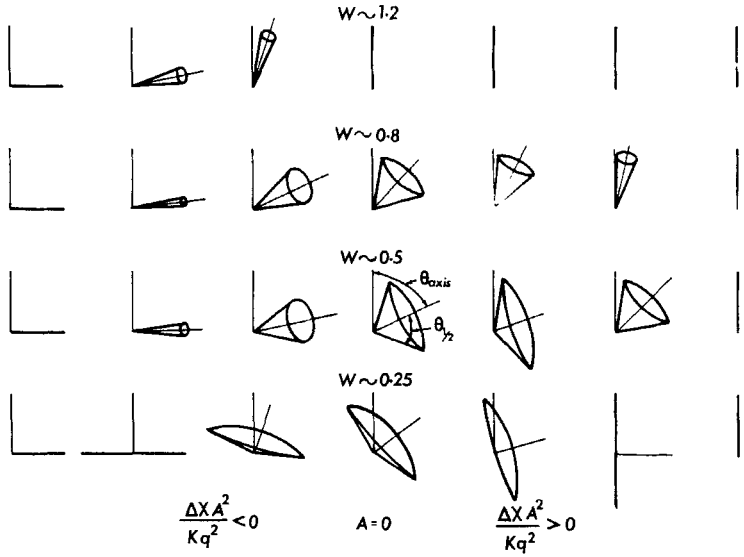

FIGURE 9 A summary of the response of the periodic cholesteric configuration to changes in thickness and applied field is indicated mnenonically by the cone formed by projecting the director fields at the midplane of the sample onto a single point. The axis of the cone makes an angle θ_{axis} with respect to the z-axis and the half-angle of the cone is $\theta_{1/2}$.

maxima and back towards zero as the field continues to increase. θ_{axis} goes towards θ_{max} of the corresponding TIC solution, which goes towards $\pi/2$.

For $W \sim 0.8$ the behavior with field is much the same except that nucleation from the homeotropic takes place with F decreasing from a positive value.

For $W \sim 0.5$ the sequence is again similar, but the maximum in $\theta_{1/2}$ occurs for $F > 0$ inasmuch as for $F = 0$ there are regions of the pattern ($\theta > \pi/2$) in which the torque from a positive applied field ($F > 0$) causes alignment further from the $\theta = 0$ axis. The transition to the homeotropic remains continuous even when the periodicity is constrained.

For $W \sim 0.25$ not only does the pattern in zero field have some regions with $\theta > \pi/2$ but in addition the cone encompasses the z-axis and a field with $F < 0$ flattens out the cone. This behavior is quite different than the previous cases. Before, a transition to the TIC solutions was possible with the periodicity constrained. Here it is not. For $F > 0$ the effect of regions with $\theta > \pi/2$ lead to the development of 360 degree Bloch walls.

This rich field of phenomena is for the case with homeotropic boundary conditions and fields vertical. It is clear that much is yet to be described for the case where the fields are in the horizontal plane. Further it remains to apply these techniques to other surface conditions.

Appendix A

The coordinate system described in Section III has computational problems when the polar angle θ is close to zero in the bulk. We then can use a coordinate system which has been rotated by $\pi/2$ about the x-axis, i.e., θ is now measured from the y-axis, while ϕ is measured from the x-axis. The director now becomes

$$\hat{n} = \hat{x} \sin\theta \cos\phi + \hat{y} \cos\theta + \hat{z} \sin\theta \sin\phi. \tag{A1}$$

The energy per unit length now becomes

$$\begin{aligned} E_l = \frac{1}{2} \iint \{ & dx\, dz (K[\theta_x^2 + \theta_z^2 + \sin^2\theta(\phi_x^2 + \phi_z^2) \\ & + 2 \sin\theta \cos\theta(\theta_x\phi_z - \theta_z\phi_x) + q^2 \\ & - 2q(\sin\phi\theta_x - \cos\phi\theta_z + \sin\theta\cos\theta(\cos\phi\phi_x + \sin\phi\phi_z))] \\ & + \Delta\chi A^2(1 - \sin^2\theta \sin^2\phi))\} \end{aligned} \tag{A2}$$

where again the term in $\chi_\perp A^2$ has been dropped since it is independent of the molecular orientation.

Minimizing the energy produces the coupled torque equations

$$\nabla^2\theta = \sin\theta\cos\theta(\phi_x^2 + \phi_z^2) + 2q\sin^2\theta(\cos\phi\phi_x + \sin\phi\phi_z) - (\Delta\chi A^2/K)\sin\theta\cos\theta\sin^2\phi \tag{A3}$$

and

$$\sin^2\theta\nabla^2\phi = -2\sin\theta\cos\theta(\theta_x\phi_x + \theta_z\phi_z) - 2q\sin^2\theta(\cos\phi\theta_x + \sin\phi\theta_z) - (\Delta\chi A^2/K)\sin\phi\cos\phi\sin^2\theta. \tag{A4}$$

The boundary conditions require $\theta = \phi = \pi/2$ at the surfaces.

Appendix B

Both coordinate systems previously described in the text have computational problems when their polar angle θ is close to zero. A better coordinate system for use on computers is the direction cosine system with the use of a Lagrange multiplier λ to ensure the unit constraint. The disadvantage of this coordinate system from a learning point of view is the difficulty in deriving any analytical limits.

In this coordinate system the director can be written as

$$\hat{n} = \hat{x}\alpha + \hat{y}\beta + \hat{z}\gamma \tag{B1}$$

with the constraint

$$n^2 = \alpha^2 + \beta^2 + \gamma^2 = 1. \tag{B2}$$

The energy per unit length becomes

$$E_l = \frac{1}{2}\iint\{dx\,dz([(\alpha_z^2 + \beta_z^2 + \gamma_z^2 + \alpha_x^2 + \beta_x^2 + \gamma_x^2 + 2(\alpha_x\gamma_z - \alpha_z\gamma_x) + 2q(\alpha\beta_z - \beta\alpha_z + \beta\gamma_x - \gamma\beta_x) + q^2] + \Delta\chi A^2(1 - \gamma^2))\}. \tag{B3}$$

The constraint can be handled by the use of the Lagrange multiplier λ (which is a function of position) producing the Lagrange energy

$$E^* = E + \iint dx\,dz\,\lambda(\alpha^2 + \beta^2 + \gamma^2) \tag{B4}$$

which is minimized producing the three coupled torque equations

$$\nabla^2\alpha = \lambda\alpha + 2q\beta_z. \tag{B5}$$

$$\nabla^2\beta = \lambda\beta + 2q(\gamma_x - \alpha_z) \tag{B6}$$

and

$$\nabla^2\gamma = (\lambda - \Delta\chi A^2/K)\gamma - 2q\beta_x \tag{B7}$$

which along with the equation of constraint, Eq. (B2), gives four equations in the four unknowns α, β, γ and λ.

At the surfaces $\alpha = \beta = 0$ and $\gamma = 1$ ensure the required homeotropic alignment.

The method of solution of these equations by finite difference techniques will be described briefly. If the grid size in both the x- and z-directions is d then Eq. (B5) can be written as

$$\frac{\diamondsuit\alpha - 4\alpha}{d^2} = \lambda\alpha + 2q\beta_z \tag{B8}$$

where $\diamondsuit\alpha$ is the sum of the four nearest neighbour α-values of the point of interest. This can be rewritten as

$$\alpha(\gamma d^2 + 4) = \diamondsuit\alpha - 2q\beta_z d^2 \tag{B9}$$

Similarly Eqs. (B6) and (B7) can be written as

$$\beta(\lambda d^2 + 4) = \diamondsuit\beta - 2q(\gamma_x - \alpha_z)d^2 \tag{B10}$$

and

$$\gamma(\lambda d^2 + 4) = \diamondsuit\gamma + ((\Delta\chi A^2/K)\gamma + 2q\beta_x)d^2. \tag{B11}$$

Squaring Eqs. (B9–B11), adding them together and making use of Eq. (B2) gives a value for $(\lambda d^2 + 4)$. This can then be used to determine the new values of α, β, and γ at the point in terms of the values at the neighbouring points from Eqs. (B9–B11). The points are calculated in sequence. This technique is iterated until a stable solution has been found.

References

1. M. J. Press and A. S. Arrott, *J. de Physique*, **37**, 387–95 (1976).
2. P. G. de Gennes, *The Physics of Liquid Crystals*, Clarendon Press (1974), 81.
3. V. Fredericks and V. Zolina, *Trans. Faraday Soc.*, **29**, 919 (1933).
4. M. J. Press and A. S. Arrott. To be published.
5. R. M. Hornreich. Private communication.
6. A. E. La Bonte, *J. Appl. Phys.*, **40**, 2450 (1969).